(CO_2 + 2-Propanol) Mixture as a Foaming Agent for Polystyrene: A Simple Thermodynamic Model for the High Pressure VLE-Phase Diagrams Taking into Account the Foam Vitrification

Marco Dondero, José Carella, Julio Borrajo

Institute of Materials Science and Technology (INTEMA), University of Mar del Plata and National Research Council (CONICET), 7600 Mar del Plata, Argentina

Received 21 February 2006; accepted 16 October 2006
DOI 10.1002/app.25658
Published online in Wiley InterScience (www.interscience.wiley.com).

ABSTRACT: The equation of state model developed by Lacombe and Sanchez (J Phys Chem 1976, 80, 2352) is used in the form proposed later by Sanchez and Stone (Polymer Blends, Vol. 1: Formulation, 2000; Chapter 2) to correlate experimental vapor-liquid equilibrium (VLE) data for the three binaries and the ternary systems. Experimental data from the binary systems carbon dioxide-isopropyl alcohol (CO_2-IPrOH), isopropyl alcohol-polystyrene (IPrOH-PS), and carbon dioxide-polystyrene (CO_2-PS) are used to calculate VLE properties for the ternary system CO_2-IPrOH-PS. Two-dimensional VLE-phase diagrams were calculated and used to describe from a thermodynamic point of view the pressure, volume, and temperature values that characterize a thermoplastic foam evolution process, from the extruder to the foaming die. For different initial mixture CO_2 + IPrOH concentrations, pressure reduction produces liquid foaming until the vitrification curve arrests the final foam volume expansion. The dependence of the vitreous transition with the system CO_2 + IPrOH concentration while foaming is represented by the Chow (Macromolecules 1980, 13, 362) equation. The calculation procedure is proposed as a design tool to reduce the amount of experimental data usually needed as a requirement previous to the design stage. © 2007 Wiley Periodicals, Inc. J Appl Polym Sci 104: 2663–2671, 2007

Key words: PS foams; phase diagrams; vitrification; thermodynamics; foaming process

INTRODUCTION

In thermoplastic polymers foam production, blowing agents selection affects process system design and optimization. CFCs will be banned for use as a foaming agent because of environmental damage effects. Hydrocarbons as propane or butane have also been used in spite of its difficult manipulation because of fire and explosion danger, but are expected to be banned in a short time.

The use of carbon dioxide (CO_2) as a blowing agent has already been established. CO_2 is not considered as a contaminating agent, and it does not leave any toxic residuals in the final product. The use of CO_2 implies modifications of the traditional foam blowing process, dramatically changing the composition, temperature, and pressure-operating conditions.

Liquid CO_2 must be injected at relatively high pressure because of its low solubility in most common thermoplastics. Furthermore, as the injected liquid CO_2 is put in contact with melts at high temperatures and pressures, it becomes a highly compressible fluid, and therefore requires suitable expensive pumps to inject it into the process equipment. Also, the CO_2 high compressibility makes exact measurement of the injected amount difficult, and requires expensive equipment. Reducing the blowing agent compressibility may allow the use of simpler and less expensive equipment.

Noncompressible liquid solvents may render suitable liquid CO_2 solutions that can be pumped with cheaper and more reliable pumps and measuring equipment. IPrOH has already been used as cosolvent in the mixture with CO_2 to make poly methylmethacrylate (PMMA) foams.[1] For the same purpose, mixtures of CO_2 and 2-hethyl hexanol have been experimentally tested as a foaming agent to produce PS foams of variable density.[2]

Taking advantage of the high solubility of CO_2 in alkyl alcohols at elevated temperatures and pressures, a homogeneous mixture of CO_2 and IPrOH was selected as the blowing agent for this work. Therefore, we must be able to predict the phase behavior of the CO_2(1) + IPrOH(2) + PS(3) ternary system at all process conditions.

Correspondence to: J. Borrajo (jborrajo@fi.mdp.edu.ar).

Journal of Applied Polymer Science, Vol. 104, 2663–2671 (2007)

Thermoplastic polymers foaming processes consist of making a homogeneous liquid solution of the blowing agent in the melt, and then demixing into a liquid and a vapor phases by lowering the pressure to induce a rapid separation of the blowing agent from the solution. The formed bubbles expand the melt, and thus structural foam is formed upon cooling. For process design and control, a complete quantitative description of the relationships existing between liquid and vapor-phase compositions, temperatures, and pressure is needed. Also, some polymer properties of interest for the process, such as viscosity and glass transition temperature, T_g, are changed by the presence of solvents and by the effect of the pressure, and these changes must be modeled.

Quantitative experimental determination of pressure–volume–temperature–composition, PVT_x, relationships for any ternary system is very expensive, mostly because of the high pressures and low CO_2 concentrations involved. Also, the PS high viscosity and high T_g add extra complications to the experimental work.

Thermodynamic equation of state (EOS) modeling was used to build a predictive design tool. The EOS developed by Sánchez and Lacombe (S–L)[3,4] was chosen because it uses only binary interaction parameters that can be calculated from experimental data found in the literature. The foundations of the S–L lattice fluid model were revisited by Sánchez and Stone (S–S)[5] showing that the configurational entropy in multicomponent systems is better represented by the Flory-Huggins model.[6] The chemical potentials for the mixture components used for this work were changed from the original S–L model,[4] as suggested by S–S.[5] For the pure components, the EOS is the same as in the S–L original model,[3] and the characteristic parameters given in the literature for pure components are used in this work for equilibrium calculations.

Application of the thermodynamic model[5] for the vapor-liquid equilibrium (VLE) calculation for the CO_2(1) + IPrOH(2) + PS(3) ternary system requires knowledge of the characteristic PVT parameters for the pure components, and experimental VLE equilibrium data for the CO_2 + IPrOH, CO_2 + PS, and IPrOH + PS binary systems. From these data, the interaction parameters for the three binary systems could be calculated with the modified thermodynamic model,[5] but the values are different from those calculated with the S–L original model. Besides, the physical meanings for all pure and binary model parameters have been clearly stated.[3–5] VLE for the CO_2 + IPrOH + PS ternary system can be estimated from these pure and binary data, assuming no extra interaction parameters are needed.

The (CO_2 + IPrOH) foaming agent dissolved in PS acts as a plasticizer, and it is expected to reduce the glass transition temperature of PS. The CO_2 + IPrOH + PS mixture is a homogeneous liquid solution at processing conditions, up to the stage previous to the decompression foam-forming process. In the decompressing stage, carried at almost constant temperature, the evaporation of the CO_2 + IPrOH mixture (mainly CO_2) starts. Evaporation of the volatile components from the compressed liquid ternary polystyrene solution causes its T_g to rise, and the foam-blowing process stops when the liquid polystyrene solution T_g reaches the process temperature. The process rate and the end of the foaming stage have been shown to influence the final morphology of the foam (foam density, cell size distribution, and open or closed cells).

To predict T_g changes with the (CO_2 + IPrOH) polymer solution contents, the model developed by Chow et al.[7] is used. The model relates T_g changes because of molecular weight, molecular size, and concentration of cosolvents, the number of lattice sites, the monomer molecular weight, and the transition isobaric specific heat increment. This model has been thoroughly tested for polystyrene solutions with several solvents.[7]

THERMODYNAMIC MODEL BACKGROUND

The S–L original model[3,4] and the S–S[5] have been developed based on the lattice-fluid theory. The material compressibility for solutions is calculated on the basis of the free volume that comes out of the total fraction of empty lattice sites. The solution free volume depends on the pure components free volumes and on the system PVT_x variables.

The EOS is expressed in terms of the system-reduced variables:

$$\tilde{\rho}^2 + \tilde{P} + \tilde{T}\left[\ln(1-\tilde{\rho}) + \left(1-\frac{1}{r}\right)\tilde{\rho}\right] = 0 \qquad (1)$$

where $\tilde{\rho} = \frac{\rho}{\rho^*}$, $\tilde{T} = \frac{T}{T^*}$, and $\tilde{P} = \frac{P}{P^*}$ are the system dimensionless variables; P, T, and ρ are the absolute real variables; and ρ^*, P^*, and T^* are the characteristic pure component parameters. The molecular size $r = r_i$ when the EOS is applied to i pure component system and $r = \bar{r}$ for mixtures. Thermodynamic variables are in dimensionless forms to help the numerical solution to converge.

For the VLE in a multicomponent mixture, the absolute variables that determine the system behavior are P, T, liquid, and vapor molar fractions of i component, x_i and y_i, and the liquid and vapor densities, ρ^l and ρ^v.

TABLE I
Characteristic Parameters and Molecular Weights for the Pure Components Used in the VLE Equilibrium Calculation for the Binary and Ternary Systems

Component	T^* (K)	P^* (MPa)	ρ^* (g/cm^3)	Ref.	M g/mol
CO_2	283	659.0	1.620	5	44.01
PrOH	420	886.6	0.972	8	60.09
PS	735	356.9	1.105	5	$2.5{\cdot}10^5$

The initial data needed for the pure components (CO_2, IPrOH, and PS) are the molecular weights M_i and the characteristic parameters T_i^*, P_i^*, and ρ_i^* found in literature.[5,8,9]

Associated parameters are the interaction energy between segment pairs of component i, $\varepsilon_{ii}^* = \frac{T^*}{k}$, the lattice site volume for the i pure component is $v_i = \frac{\varepsilon_{ii}^*}{P^*}$, and the component i molar size, $r_i = \frac{M_i}{\rho_i^* v_i}$.

Table I shows pure components characteristic parameters and molecular weights values.

The ''one-fluid'' hypothesis is usually applied to represent the PVT behavior of multicomponent system and the existence of a unique fluid with its own characteristic parameters is assumed. This approximation is widely used when LLE and VLE calculations are usually applied to any EOS, and combination rules for the characteristic parameters T_i^*, P_i^*, ρ_i^*, or the equivalent associated parameters ε_{ii}^*, v_i, and r_i must be defined. Interaction energies are defined by the geometric rule of Berthelot, and thus an empirical correction factor z_{ij} is included to account for the deviations from this rule in real systems. Binary interaction energies ε_{ij}^* between unlike are calculated as:

$$\varepsilon_{ij}^* = z_{ij}\left(\varepsilon_{ii}^*\varepsilon_{jj}^*\right)^{0.5} \tag{2}$$

From Berthelot's rule, a dimensionless Flory-Huggins interaction parameter χ_{ij} is defined as:

$$\chi_{ij} = \left(\varepsilon_{ii}^* + \varepsilon_{jj}^* - 2\varepsilon_{ij}^*\right)\Big/ kT \tag{3}$$

Some experimental characteristics of the binary systems behavior, valid for the P and T operation ranges covered for this work, are used to simplify calculations. For the CO_2 + PS binary system, the composition of the gaseous phase is almost pure CO_2 because PS is a nonvolatile component.[9] For the IPrOH + PS pair, the composition of the gaseous phase is almost pure IPrOH because of the same reason as in the other binary systems. For the CO_2 + IPrOH binary system, the composition of the gaseous phase is almost pure CO_2[10] at low temperatures, but at the high process temperatures, the IPrOH gaseous concentrations are not small. Because of these assumptions, the liquid phase of the CO_2 + IPrOH + PS ternary system at the VLE equilibrium will contain the three components, while the vapor phase will be formed by the CO_2 + IPrOH mixture.

The liquid and gas phase densities and concentrations for all binary and ternary systems, at the process P and T, are calculated by simultaneously solving the EOS and chemical potential equations applied to the gaseous and liquid equilibrium phases.

The EOS is given by eq. (1) and the chemical potential equation is given by eq. (4) for a pure component vapor phase.

$$\frac{\mu_i^v}{kT} = \ln(\tilde{\rho}^v) + r_i\left[-\frac{\tilde{\rho}^v}{\tilde{T}_i} + \frac{\tilde{P}_i\tilde{v}^v}{\tilde{T}_i} + (1-\tilde{\rho}^v)\ln(1-\tilde{\rho}^v)/\tilde{\rho}^v\right] \tag{4}$$

The chemical potentials for the components in the liquid or vapor multicomponent phases are given by eq. (5), as proposed by Sanchez and Stone.[5] For example, for the ith component in the liquid phase is,

$$\frac{\mu_i^l}{kT} = \ln\left(\tilde{\rho}^{\,l}\phi_i^l\right) + \left(1 - \frac{r_i}{\overline{r}^l}\right) + r_i\tilde{\rho}^{\,l}\left[\sum_{j=1}^{m}\phi_j^{*l}\chi_{ij} - \sum_{j=1}^{m}\sum_{i<j}\phi_i^{*l}\phi_j^{*l}\chi_{ij}\right] + r_i\left[-\frac{\tilde{\rho}^{\,l}}{\tilde{T}_i} + \frac{\tilde{P}_i\tilde{v}^l}{\tilde{T}_i} + (1-\tilde{\rho}^{\,l})\ln(1-\tilde{\rho}^{\,l})/\tilde{\rho}^{\,l}\right] \tag{5}$$

Characteristic parameters for each composition mixture are calculated as follows, for the liquid phase:

$$\text{Characteristic density:}\qquad \rho^{*l} = 1\Big/\sum_{i=1}^{m}\frac{m_i^l}{\rho_i^*} \tag{6}$$

$$\text{The } i^{\text{th}} \text{ component mass fraction:}\qquad m_i^l = \frac{x_i^l M_i}{\sum_{j=1}^{m} x_j^l M_j} \tag{7}$$

$$\text{Characteristic pressure:}\qquad P^{*l} = \varepsilon^{*l}/\overline{v}^l \tag{8}$$

$$\text{Characteristic temperature:}\qquad T^{*l} = \varepsilon^{*l}/k \tag{9}$$

Characteristic energy:

$$\varepsilon^{*l} = \sum_{i=1}^{m}\phi_i^{*l}\varepsilon_{ii}^* - \sum_{j=1}^{m}\sum_{i<j}\phi_i^{*l}\phi_j^{*l}kT\chi_{ij} \tag{10}$$

$$\text{Average molar hard core volume:}\qquad \overline{v}^{\,l} = \sum_{i=1}^{m}\phi_i^{*l}v_i \tag{11}$$

$$\text{Species average molecular weight:}\qquad \overline{M}^{\,l} = x_i^l M_i \tag{12}$$

$$\text{Solution average molar size:}\qquad \overline{r}^l = \sum_{i=1}^{m} x_i^l r_i \tag{13}$$

$$\text{The } i^{\text{th}} \text{component volume fraction:}\qquad \phi_i^{*l} = x_i^l\,\frac{r_i}{\overline{r}^l} \tag{14}$$

Reduced specific volumes for vapor and liquid phases:

$$\tilde{v}^v = 1/\tilde{\rho}^v \qquad \tilde{v}^l = 1/\tilde{\rho}^l \tag{15}$$

Validation of the calculation hypothesis and determination of z_{ij} binary interaction parameter

On the basis of the above-mentioned hypothesis that the vapor phases for the CO_2 + PS and IPrOH + PS binary systems consist of pure CO_2 gas and IPrOH gas, respectively, the equations for the LVE calculations in these systems are

$$P^v(T) = P^l(T, \phi_i^{*l}) \tag{16}$$

$$\mu_i^v(P, T) = \mu_i^l(P, T, \phi_i^{*l}) \tag{17}$$

For the CO_2 + IPrOH system, the assumtion that vapor phase is constituted by almost CO_2 is valid at low temperatures only as shown in Figure 1. For high temperature calculations, we must take into account that IPrOH concentration in the vapor phase is not meaningless. As a consequence, the equations for the VLE calculations of this binary are

$$P^v(T, \phi_i^{*v}) = P^l(T, \phi_i^{*l}) \tag{18}$$

$$\mu_i^v(P, T, \phi_i^{*v}) = \mu_i^l(P, T, \phi_i^{*l}) \tag{19}$$

Thermodynamic model predictions were compared with the experimental results for the three binary systems and the empirical interaction parameters z_{ij} were calculated for each one of them.

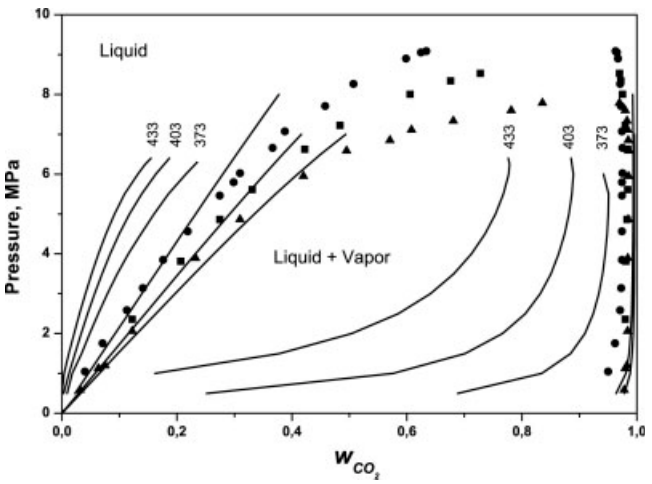

Figure 1 VLE-phase diagram for CO_2 + IPrOH binary system. Lines were calculated with the thermodynamic model. Symbols correspond to experimental data from Ref. 10: ▲, 313 K; ■, 323 K; and ●, 333 K.

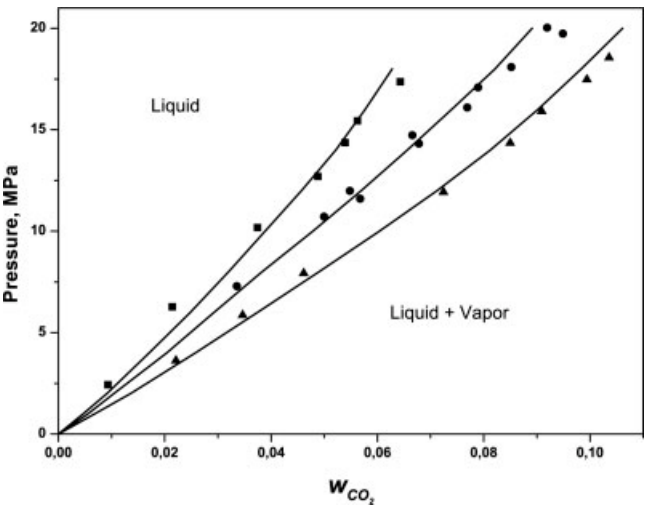

Figure 2 VLE-phase diagram for the CO_2 + PS binary system. Lines were calculated from the thermodynamic model. Symbols correspond to experimental data from Ref. 9: ■, 373 K; ●, 413.2 K; and ▲, 453.2.2 K.

CO_2 + IPrOH binary system

Experimental data from Ref. 10 were used to calculate the z_{ij} interaction parameter for L–V equilibrium conditions. Figure 1 shows the curves for several operation temperatures. Experimental results in Figure 1 show that gas phase is mostly CO_2 ($y_{CO_2} \cong 1$) at low temperatures, but at high enough temperatures, the vapor phase IPrOH concentrations increase and the eqs. (18) and (19) must be used to fit the experimental results. Interaction parameter z_{ij} is the fitting variable in this calculation, and its value depends lightly on the temperature as $z_{12} = 0.9977 + 0.000333T$.

CO_2 + PS binary system

Experimental data from Ref. 9 were used to calculate the interaction parameter, z_{13}, for the VLE calculations. Figure 2 shows curves for several operation temperatures. It was found that the values for the interaction parameter z_{13} must be a function of temperature. The whole set of calculated curves show good agreement with available experimental data when the values of the interaction parameter z_{13} are correlated by a linear equation as $z_{13} = 1.1276 - 0.0005T$.

IPrOH + PS binary system

Experimental VLE data from ref. 11 were used to calculate the interaction parameters z_{23} of this binary system. Figure 3 shows the experimental data expressed in the form of Henry's law. The Henry's constants ($\boldsymbol{H}$ = 257.1 bar at 435 K)[11] were used to calculate the experimental data to be fitted with the

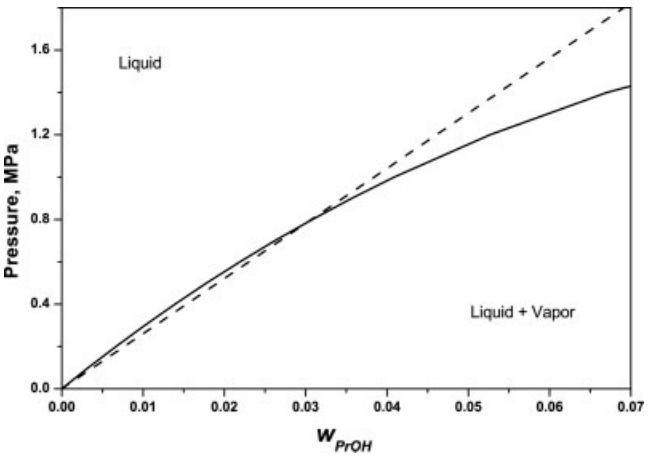

Figure 3 VLE-phase diagram for the IPrOH + PS binary system. Broken line represents the Henry's law fit for the experimental results. Henry's constant was taken from Ref. 11. Continuous line was calculated with the thermodynamic model.

thermodynamic equations. The best fit for the thermodynamic model was found for an interaction parameter value of $z_{23} = 1.001$.

GLASS TRANSITION TEMPERATURES OF CO_2 + PS, IPrOH + PS, AND CO_2 + IPrOH + PS LIQUID SOLUTIONS

The general correlation developed by Chow et al.[7] was used for this purpose. The correlation function is expressed in terms of the dimensionless variables θ and β, which depend on the diluents molecular weight, the mass fraction, and polymer parameters:

$$\ln\left(\frac{T_g}{T_{g0}}\right) = \beta\,\{(1-\theta)\,\ln(1-\theta) + \theta\,\ln(\theta)\} \qquad (20)$$

$$\theta = \frac{M_p}{\lambda M_d}\,\frac{w}{1-w} \qquad (21)$$

$$\beta = \lambda R/M_p\,\Delta C_{pp} \qquad (22)$$

where M_p is the PS repeating unit molecular weight, λ is the lattice coordination number, M_d is the diluent (CO_2 + IPrOH) average molecular weight, w is the diluent mass fraction in the liquid polymer solution, and ΔC_{pp} is the excess transition isobaric specific heat of the polymer. The polystyrene has the following properties: M_p = 104.15 g/mol, λ = 2, $M_p\,\Delta C_{pp}$ = 6.45 cal/(mol K), and pure PS T_g^0 = 373 K. Calculated T_g for all system compositions are obtained from eq. (22). Results shown as a dash line in Figure 4 have been calculated for different total masses of the foaming agent mixture, CO_2 + IPrOH, with a fixed mass ratio CO_2/IPrOH of 2/3.

For comparison purposes, T_g values for the CO_2 + PS binary solutions are also represented with a continuous line in this figure, and with a dotted line for the IPrOH + PS liquid binary solutions. A dashed line is located between the above-mentioned two lines, showing the vitrification behavior for the CO_2 + IPrOH + PS ternary liquid mixture. The abscissa represents the solvent mass fraction for each PS liquid solutions. It can be observed that IPrOH solvent alone causes the higher T_g values, because IPrOH alone has a higher molecular weight than the CO_2 or the CO_2 + IPrOH mixtures. The dash–dot curve represents the T_g of the CO_2 + IPrOH + PS liquid solution as a function of its CO_2 mass fraction. For a given CO_2 concentration, the CO_2 + IPrOH + PS ternary liquid has a lower T_g than the CO_2 + PS one. As a consequence, comparing the binary CO_2 + PS solutions with CO_2 + IPrOH + PS ternary, both having the same CO_2-foaming capacity (equal CO_2 concentration), the practical use of the ternary is advantageous for the foaming process because of the lower T_g and reduced liquid viscosity.

Most polymers glass transition temperatures increase with hydrostatic pressure.[12] The T_g increase depends mainly on the polymer chemical structure, and it is low for PS (0.25 K/MPa). We assume that the foaming process occurs at low pressure values, typically between 1 and 10 MPa. Thus, the T_g for the foaming liquid will depend mainly on the diluents concentration.

COMPARISION BETWEEN CO_2 + PS AND CO_2 + IPrOH + PS FOAMING SYSTEMS

CO_2 + IPrOH + PS ternary system

To apply the thermodynamic model to this three-component system, the following assumptions were applied: (1) deviations from Berthelot rule behavior

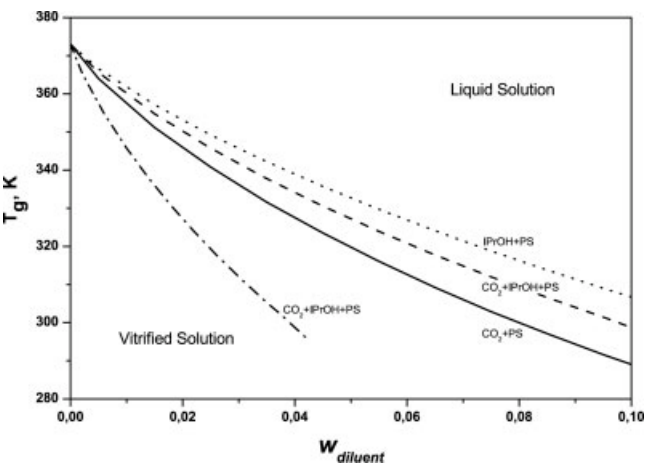

Figure 4 Vitreous temperature for the binary and ternary systems as functions of diluents mass fraction. Lower CO_2 + IPrOH + PS solutions as a function of w_{CO_2}.

for the whole system can be represented by the summation of the three binary systems contributions already calculated as binary interaction parameters z_{ij}; (2) the liquid phase contains the three components, CO_2 + IPrOH + PS while the vapor phase is made up of the volatile components binary mixture CO_2 + IPrOH.

The VLE-phase diagram for this system has been calculated only for low foaming agent mixture concentrations, because of two reasons: (1) foaming processes require relatively low CO_2 mass fractions because of its large volume contribution to the expansion of the vapor phase during foaming; (2) the assumption used to estimate the vapor-phase composition is expected to be more realistic for low (CO_2 + IPrOH) foaming agent mixture concentration, because the fitting behavior of the z_{ij} interaction parameters is better in this concentration range.

The LV thermodynamic equilibrium was calculated by simultaneously solving the three-equations system:

$$P^v(T, \phi_i^v) = P^l(T, \phi_i^l) \tag{23}$$

$$\mu_2^v(T, P, \phi_i^v) = \mu_2^l(T, P, \phi_i^l) \tag{24}$$

$$\mu_1^v(T, P, \phi_i^v) = \mu_1^l(T, P, \phi_i^l) \tag{25}$$

where $i = 1, 2, 3$ stands for CO_2, IPrOH, and PS, respectively.

VLE-equilibrium-phase diagrams for the ternary CO_2 + IPrOH + PS system, calculated at three temperatures, are shown in Figure 5 as full lines. These calculations have been done for a foaming agent mixture with a CO_2/IPrOH mass ratio of 2/3. The CO_2 is injected at the extruder injection port as a CO_2/IPrOH liquid solution with a mass ratio of about 2/3. As the system is maintained at high enough pressure, it is expected that this mass ratio will stay constant in the ternary liquid solution until the beginning of the foaming stage at the liquid mixture bubble point.

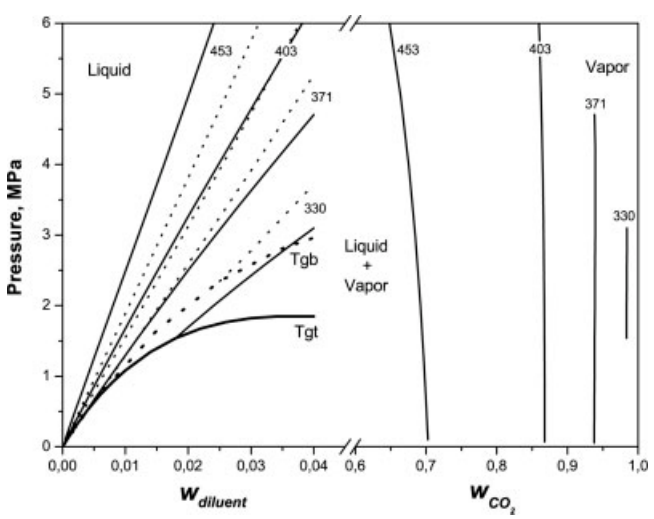

Figure 5 VLE-phase diagrams for the ternary CO_2 + IPrOH + PS and binary CO_2 + PS systems. Thin continuous lines represent the ternary, and broken lines represent the binary. Thick continuous line represents vitrification temperature T_gt for the ternary and the thick broken line represents the T_gb for the binary.

VLE lines for the binary (CO_2 + PS) system, calculated for the same temperatures, are also shown in Figure 5 as dashed lines. Predicted behavior for the foaming process, using only CO_2 as a foaming agent, can be compared with the foaming process that uses (CO_2 + IPrOH) as a foaming agent mixture.

Vitrification lines for the ternary and for the binary-foaming systems were calculated converting the corresponding T_gw lines of Figure 4 in P_gw lines in Figure 5. To do that, each T_gw point was converted to a P_gw equivalent point by using the thermodynamic eqs. (23–25) for the ternaries and eqs. (18) and (19) for the binaries.

From a thermodynamic point of view, there are some significant differences in the equilibrium P, T, w process variables values in the usual range of CO_2-foaming agent concentrations. The major differences observed between both foaming systems, represented in Figure 5, are (1) a vapor phase formed by CO_2 and IPrOH is observed for the ternary foaming system at high temperatures; (2) at low temperatures, the cosolvent IPrOH concentration in the vapor phase decreases, and that of the CO_2 increases to values higher than 95% at 343 K; (3) the VLE isotherms for the CO_2 + PS are placed above those corresponding to the respective ternary for the lower temperature isotherms; (4) when the system temperature increases, the position of the VLE isotherms are inverted and the binaries are below the ternaries; (5) the inversion temperature is near 400 K, as can be observed in Figure 5; (6) at low temperatures, the VLE equilibrium isotherms for the binary and the ternary systems are interrupted by the vitrification lines at different final concentrations. The observed inversion in the relative positions of the binaries and ternaries VLE lines is caused by the change of the interaction parameters z_{12} and z_{13} with temperature, z_{12} decreases and z_{13} increases when temperature increases.

From a practical point of view, two important conclusions can be drawn at this point: (1) the foam bubbles at high temperatures are made out of the two gases CO_2 and IPrOH in a appreciable amount, the bubbles CO_2 content greatly increases when the temperature is reduced, (2) low temperatures at the die exit can interrupt the foaming process because the liquid mixture T_g is reached, and this will occur earlier in the binary CO_2 + PS foaming system because of its high T_g.

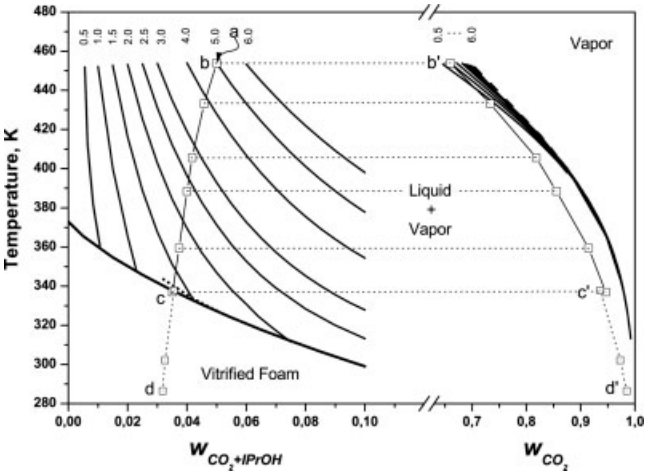

Figure 6 Foaming trajectory in a T versus w VLE-phase diagram for CO_2 + IPrOH + PS foaming system at different constant pressures: abcd – foaming trajectory is in the liquid phase; b, c, d – foaming trajectory is in the gaseous phase.

FOAMING PROCESS ANALYSIS

Foaming process path in a *T-w* graph

Figure 6 presents a transformation diagram that contains all the relevant information for a thermodynamic analysis of the foaming process. This figure has two parts, a left-side part representing the ternary liquid phase *PTw* behavior, where *w* represents the liquid global cosolvents mass fraction (CO_2 + IPrOH), and a right-side part representing the vapor phase *PTw* behavior, where *w* represents the CO_2 mass fraction of the binary-vapor phase. The thick continuous line in the left-side part has the same meaning as the vitrification line shown in Figure 5: at this line *PTw* conditions the foaming process is arrested. The nine lines in the left-side part of the graph represent the temperature, pressure, and composition, *TPw*, for the liquid equilibrium phases, at the bubble point, for nine fixed operation pressure values. These lines end at the T_g line. The nine lines in the right part represent the vapor phases in equilibrium with the corresponding liquid phases placed at the left-side part.

Operating pressures are considered suitable only if all the injected CO_2 + IPrOH solutions remain in a stable CO_2 + PrOH + PS homogeneous solution, all the way up to the decompression stage at the foaming die. In the continuous foaming process, the homogeneous liquid (CO_2 + IPrOH + PS) ternary solution is transported from the extruder mixer exit to the foaming die at high pressure and temperature. Upstream the foaming die, the solution is usually in the vicinity of 450 K and 10 MPa, represented by a point (*a*) with $w_{CO_2+IPrOH} = 0.05$, at 453 K above 5 MPa. Actually, point (*a*) ought to be placed at the same *T-w* position as point (*b*), but at higher pressure. At the foaming die, a sudden cross section enlargement causes a rapid pressure drop from (*a*) to (*b*), and the ternary liquid solution remains as a homogeneous liquid and its concentration is unchanged. At point (*b*), the ternary liquid solution reaches the bubble point, and VLE equilibrium is developed between the liquid ternary phase, marked by the point *b*, and a vapor binary phase, marked by the point *b*′. The line (*bb*′) represents the true initial stage where the foaming process starts from the liquid (CO_2 + IPrOH + PS) ternary solution, and the merging (CO_2 + IPrOH) gaseous phase shows up for the first time. The calculated pressure for the tie line (*bb*′) is 5 MPa. The liquid phase trajectory from point (*b*) to point (*c*), and its conjugate vapor phase trajectory from point (*b*′) to point (*c*′) represent the actual foaming process. The (CO_2 + IPrOH) vapor mixture bubbles start coming out of the ternary liquid solution, and along the foaming line (*bc*) the gas bubbles nucleation, growing, and coalescence takes place simultaneously, increasing the gas phase volume responsible of the foaming process. During this foaming process, the vapor composition becomes richer on the most volatile CO_2 gas, with smaller but not meaningless amounts of IPrOH gas. The liquid phase becomes poorer in the blowing mixture, where global concentration is smaller than the original 0.05 at the starting point *b*. The molar cosolvents ratio in the remaining liquid solution along the *bc* trajectory is lower than the original 2/3 one, because CO_2 is preferentially segregated to the vapor phase. The continuous reduction of the cosolvents global concentration in the liquid phase causes the liquid T_g to increase continuously as described by the Chow et al.[7] model in Figure 4. The vitrification line along the foaming trajectory is a characteristic feature for each trajectory, because the cosolvent concentration and its CO_2/IPrOH ratio change continuously and in a particular way while foaming. The $T_g w$ line for the selected trajectory is represented by the short-dashed thick line passing through the *c* point. The foaming process continues along the line (*bc*), where the pressure and temperature are reduced, until the vitrification of the liquid phase takes place at point (*c*) on its own T_g line. At this point, the foaming process is arrested because the foam walls become glassy. At this condition, the foam volume and the mole number of the gaseous cosolvents phase reach the final values. The foam volume is determined by the volume of the vitrified solid phase plus the volume of the bubbles gas phase. The cumulate global mole number and concentration of the equilibrium liquid and vapor phases during the foaming process are described by each tie line along the trajectories (*bc*) and (*b*′*c*′) lines. Between the (*bc*) line in the liquid phase and the (*b*′*c*′) line in the vapor phase, some tie

lines are shown in Figure 6, joining the two equilibrium phases during the foaming process. Assuming thermodynamic equilibrium is reached, the volume and the mole number in both equilibrium phases could be obtained by solving simultaneously the mass balance and the equilibrium thermodynamic equations during the foaming process.

Subsequent cooling will take the system from (cc') *PTw* conditions to the final conditions of the store room, point *d*. The pressure reduction during this step originates the driving force for CO_2 and IPrOH desorption from the whole-foamed system. This transformation takes place from the gas phase bubbles and from the glassy bubbles walls, but without any noticeable foam-morphology change. The time for CO_2 and IPrOH mass loss during the foam storage at room temperature can be extended over a long period of 1–2 years.[2]

Vitrified solid foam is the final expected behavior for the obtained material.

If vitrification could take place at lower temperatures, the foaming process could continue as represented by the (cd) and ($c'd'$) lines, increasing markedly the final foam volume. This volume and the mole number of cosolvents in both equilibrium phases could be obtained too, as was previously mentioned. If the new T_g is close to ambient temperature, this foam could show a ''soft rubbery'' final behavior.

Foam volume and gaseous mole number evolution

Figure 7 shows the calculated gaseous volume and mole number evolution along the foaming trajectory in a pressure versus foam volume representation at the left-side vertical axis, and gaseous mole number versus foam volume at the right-side vertical axis.

The foam volume and the gaseous mole number for each tie line along the foaming trajectory (bc)–($b'c'$) in Figure 6 were calculated from the mass balance equations and the thermodynamic model. The calculated vapor and liquid phases equilibrium parameters at the T_g condition on the foaming trajectory are $P = 0.517$ MPa, $T = 332.4$ K, $n_v = 0.353$, $x_1 = 0.2098$, $x_2 = 0.7841$, $y_1 = 0.9610$, $\rho_1 = 1039.6$ g/L, and $\rho_v = 8.4756$ g/L. These thermodynamic results can be used for the foam final volume calculation. The equations to be used for the calculation are

$$\begin{aligned} V_F &= V_l + V_v \\ V_l &= (1 - n_v).[x_1M_1 + x_2M_2 + (1 - x_1 - x_2)M_3]/\rho_l \\ V_v &= n_v.[y_1M_1 + (1 - y_1)M_2]/\rho_v \end{aligned} \tag{26}$$

The results for the calculated volumes are $V_l = 1.0044$ L; $V_v = 1.8433$ L and the foam volume is $V_F = 2.8477$ L. At room temperature, this is a vitreous material poorly foamed. These equations were used to calculate the evolution of the foam volume on each tie line during all the foaming process along the (bc)–($b'c'$), these values are represented in Figure 7 with the thick full line. If vitrification restrictions were not present, the foaming process should continue down to room temperature, and final foam volume could increase to higher values, of the order of 10 L, as shown by the discontinuous lines in Figure 7.

Other trajectories with different initial mass fractions of the blowing mixture w or different mole ratios of CO_2/IPrOH for the blowing agent should give foams with different final volumes.

In this thermodynamic analysis, the rate of molecular diffusion is not taken into account but it could be expected that important diffusion molecular restriction for the vapor-phase separation during foaming could be present. In this context, the thermodynamic calculation predicts ''a maximum'' for the foaming process performance.

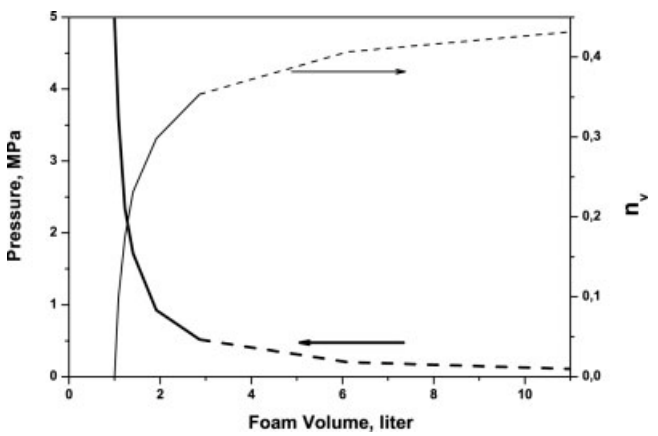

Figure 7 Evolution of the foam pressure P, volume V, and gaseous mole number n_v properties during foaming.

CONCLUSIONS

The S–L lattice fluid theory revisited by Sánchez and Stone gives simpler and accurate calculation equations for the VLE-equilibrium analysis in polymer systems, and the calculated results fit well experimental binary data on the diluted concentration range. Once the thermoplastic polymer and the foaming agent mixture to be used have been chosen, a suitable solution method can be selected and adjusted to solve the S–L EOS model.

The inclusion of IPrOH cosolvent in the foaming agent mixture introduces changes in the thermodynamic behavior, when compared with the simpler binary foaming system (CO_2 + PS) that ameliorate the operation requirements for the process equipment.

Transformation diagrams P versus w and T vs. w give a realistic and qualitative thermodynamic view for ternary systems foaming, even while the actual values of some process variables during foaming can differ slightly from thermodynamic equilibrium.

Three-dimensional graphs can be easily build from two-dimensional graphs like Figures 5 and 6, but we understand that two-dimensional graphs are quite easier to follow.

Based only on some experimental thermodynamic data information about binary systems, valuable results can be gathered to be used as preliminary design tools for

1. calculations for adequate extruder and die operation pressures and temperatures.
2. quantitative calculation of amount of foaming agent that can be safely dissolved and processed.
3. selection of the most suitable solvent to be used, in terms of solubility and T_g decrease for the ternary system.
4. foaming dies accurate design, using the thermodynamic equilibrium data together with a suitable viscous flow simulator.[13]

References

1. Moulinié, P.; Gendron, R. Presented at ANTEC Proceedings 1841–1946, Orlando, FL, May 7–11, 2000.
2. Louis, E.; Daigneault, Gendron, R. Presented at ANTEC Proceedings 1936–1940, Orlando, FL, May 7–11, 2000.
3. Lacombe, R. H.; Sanchez, I. C. J Phys Chem 1976, 80, 2552.
4. Lacombe, R. H.; Sanchez, I. C. J Phys Chem 1976, 80, 2568.
5. Sánchez, I. C.; Stone, M. T. In Polymer Blends, Volume I: Formulation; Paul, D. R., Bucknall, C. B. Eds.; Wiley: New York, 2000; Chapter 2.
6. Flory, P. J. Principles of Polymer Chemistry; Cornel University Press: Ithaca, NY, 1953.
7. Chow, T. S. Macromolecules 1980, 13, 362.
8. Kiska, M. B.; Meilchen, M. A.; McHugh, M. A. J Polym Sci 1988, 36, 583.
9. Sato, Y.; Yurugi, M.; Fujiwara, K.; Takishima, S.; Masuota, H. Fluid Phase Equilib 1996, 125, 129.
10. Startmann, A.; Schweiger, G. Presented at Conference Proceeding, Topic 12, Fourth European Congress of Chem Engineering, Granada, Spain, September 2003.
11. Wohlfarth, C. Vapor Liquid Equilibrium Data of Binary Polymer Solutions, Elsevier Science B. V.: 1994; Chapter 4, p 772.
12. Peyser, P. In Polymer Handbook, 3rd ed.; Brandrup, J.; Immergut, E. H., Eds.; Wiley-Interscience: New York, 1989.
13. Han, X.; Koelling, W.; Tomasko, D.; Lee, J. SPE Antec Tech Pap 2000, 46, 1857.